

Second-harmonic stabilization of a bulk photonic resonator

Lindell M. Williams^{1,2,*}, Grant M. Brodnik¹, and Scott B. Papp^{1,2}

¹Time and Frequency Division, National Institute of Standards and Technology, Boulder, CO 80305, USA

²Department of Physics, University of Colorado, Boulder, CO 80309, USA

The resonant modes of optical cavities provide a powerful resource for laser-frequency stabilization, underpinning high-precision metrology and coherent signal generation. Photonic resonators in which the optical mode propagates through material offer a compact alternative to vacuum Fabry-Perot cavity systems, but their performance is limited by sensitivity of the material to the ambient environment. In this work, we explore second-harmonic (SH) stabilization, which exploits the interplay of a dispersive mode structure against the strict energy conservation of second-harmonic generation. Operationally, we use two, 1550 nm lasers to PDH-detect octave-spaced resonant modes of an ultra-high-Q photonic resonator with one laser frequency-doubled to 775 nm. Under SH stabilization, the microwave frequency offset between the 1550 nm lasers, which we refer to as the SH signal (f_{SH}) maps the absolute frequency of the 1550 nm laser to an electronic signal. We characterize this mapping through comparison of the absolute optical frequency inference provided by f_{SH} to an out-of-loop optical measurement, and our results suggest f_{SH} accurately proxies frequency drift. We evaluate the sensitivity and noise floor of this technique, considering contributions from laser locking and bulk material properties, and conclude that f_{SH} is sufficiently sensitive to enhance long-term laser-frequency stability with respect to the resonator. These results demonstrate SH stabilization as a useful technique that infers absolute drift, thereby enabling the increased stability of future compact, precision frequency references.

1 Introduction

Optical cavities play a fundamental role in precision metrology, stabilizing laser frequency for applications such as optical atomic clocks [1], pristine microwave signal generation [2], and communications [3]. Lasers locked

to high-finesse, Fabry-Perot cavities feature ultranarrow linewidths and reduced frequency drift [4, 5, 6, 7], representing the state-of-the-art in short-term stability. The complicated implementation of these cavities, involving optics, vacuum, and active and passive isolation [8], have motivated new designs and integration. Photonic resonators in which light propagates through material offer advantages in compactness for applications including gas sensing [9] and geodesy [10]. These devices span a variety of form factors, including whispering-gallery mode resonators [11, 12, 13], photonic waveguide rings [14], and photonic Fabry-Perot resonators [15, 16, 17], which enable ultrahigh quality factors for narrow < 20 Hz laser linewidth. However, such resonators are limited in terms of material availability and volume for enclosure engineering. As a result, compact resonators encounter thermal noise and drift from material sensitivity to ambient exposure, ultimately reaching a thermorefractive-noise-limited linewidth and long-term temperature-induced drift. Indeed, realizing the potential of compact resonators that maintain relatively narrow linewidth requires novel methods of reducing frequency drift.

Record-low frequency drift in optical cavity systems is often achieved by decoupling optical fields from environmental perturbations to reduce resonator sensitivity. Engineered enclosures isolate Fabry-Perot cavities, utilizing vacuum and thermal controls—often at cryogenic temperatures [18]—to create a low-noise environment [4, 5, 6, 7]. Vacuum [17], mono-crystalline materials [4, 6], and Fabry-Perot materials and photonic resonators operated at expansion nulls [19, 20, 21] all offer compelling options for increased stability. In compact resonators, where size and material constraints limit the use of these techniques, active stabilization based on optical thermometry has been explored. Thermometry utilizing orthogonal polarization mode families has been demonstrated in whispering-gallery mode resonators [22, 23, 24, 25] and photonic waveguide resonators [26]. In whispering-gallery mode resonators, thermometry using a laser and its second harmonic has also been explored [27]. However, the complex geometry of whispering-gallery modes can lead to poor correlation between stabilized mode temperature

*lindell.williams@colorado.edu

and absolute frequency stability. With relatively simple geometry and design and demonstrated performance in short-term stability [15], Fabry-Perot photonic resonators offer an as-of-yet underexplored platform for frequency-drift measurement, using optical thermometry.

We introduce second-harmonic (SH) stabilization, which measures frequency drift in a resonator by balancing dispersion across octave-spaced modes against energy conservation in second-harmonic generation (SHG). For a concrete model of SH stabilization, we consider the mode structure of a dispersive resonator with mode indices, m , such that $\nu(m) = \frac{mc}{2n(\nu)L}$, where L is the resonator length and $n(\nu)$ is the refractive index at frequency ν . Performing SH stabilization on a resonator yields a microwave frequency SH signal,

$$f_{\text{SH}} = \nu_1 - \frac{1}{2}\nu_2 = \nu_1 \left(1 - \frac{1}{2} \frac{m_2}{m_1} \frac{n(\nu_1)}{n(\nu_2)} \right), \quad (1)$$

where ν_1 is a resonant frequency at the fundamental and ν_2 is the resonant frequency nearest to its second harmonic ($\nu_2 \approx 2\nu_1$). We note that a small change in f_{SH} , Δf_{SH} relates to a corresponding change in absolute resonant frequency, $\Delta\nu_1$, by the total variation of Eq. 1, $\Delta f_{\text{SH}} = (\frac{df_{\text{SH}}}{d\nu_1})\Delta\nu_1$. Importantly, f_{SH} is an intrinsic property of the resonator's dispersive mode structure; once the fundamental mode, m_1 , is selected, the corresponding second-harmonic mode, m_2 , is uniquely defined. Therefore, f_{SH} depends predominantly on resonator material properties, including the frequency-dependent refractive index and thermo-optic coefficient.

Here, we explore SH stabilization in an ultra-high-Q photonic resonator. We probe f_{SH} by use of the heterodyne of two lasers; one laser is PDH-locked to the resonator at the fundamental wavelength (1550 nm), and the second is frequency-doubled and PDH-locked at the second harmonic (775 nm). By the temperature dependence of f_{SH} , we measure $df_{\text{SH}}/d\nu_1$, which is consistent with the reference thermo-optic and dispersive properties of the resonator material. Second-harmonic stabilization relies on precise detection of resonator modes, so we analyze the limits of the technique set by both fundamental and excess technical noise in the laser locks. We explore the limits for inferring drift with f_{SH} and find it can accurately infer drift to the Hz/s level, supporting a three order of magnitude improvement over the free-running photonic resonator. These results establish SH stabilization as a viable method to enhance long-term frequency stability in compact dispersive resonators.

2 Experimental description

Figure 1 presents our experiment with SH stabilization, using a Fabry-Perot photonic resonator. The device is a

2.54 cm long, monolithic, fused silica resonator [15, 16] (Fig. 1a, right) with a plano-convex geometry and a Q of approximately 1 billion. The resonator is housed in a teflon enclosure designed to provide passive thermal and vibration isolation [15]. The resonator and its housing are further enclosed in a small box equipped with PID-controlled resistive heaters set 15°C above ambient temperature to impose a coarse level of thermal stability. We experimentally realize SH stabilization, locking two lasers to the resonator at a given frequency and its second harmonic to measure f_{SH} (Fig. 1a, left). The first laser is directly locked to a resonant mode with frequency ν_1 , corresponding to 1550 nm, using the Pound-Drever-Hall (PDH) scheme [28]. A second laser at nearly the same frequency is frequency doubled by use of a waveguide-coupled SHG crystal (periodically poled lithium niobate) and locked to an optical mode with resonant frequency ν_2 (775 nm). By mixing the two lasers on a photodiode, the heterodyne beat, $\nu_1 - \nu_2/2$, realizes f_{SH} as in Eq. 1. We illustrate this definition in Fig. 1b, showing that the dispersive mode spectrum defines f_{SH} for a specific fundamental mode and its corresponding second-harmonic mode. We use a commercial stabilized laser with drift of ~ 0.1 Hz/s as a reference (ν_{ref} , 1550 nm) for out-of-loop characterization of our photonic resonator.

Figure 1c shows our calibration of the scaling factor between fluctuations in f_{SH} and fluctuations in ν_1 . We simultaneously record f_{SH} and the out-of-loop reference heterodyne for up to 10,000 s, quantifying Δf_{SH} and $\Delta\nu_1$ by subtracting the initial frequency from subsequent data. In Fig. 1c, we calibrate by fitting the scaled f_{SH} fluctuations (black line) to resonant frequency fluctuations quantified with the reference heterodyne (green line), finding that the residual is minimized with a scaling of $\Delta f_{\text{SH}} = \frac{1}{-48.7}\Delta\nu_1$. In this work, we treat the scaling factor as constant over time and apply this calibrated scaling to all subsequent inferences of ν_1 from f_{SH} .

Imprecision and inaccuracy of the resonator material properties, including index of refraction and thermo-optic coefficient, and environmental couplings reduce the absolute accuracy of ν_1 inferred from f_{SH} . Nonetheless, we leverage the relationship presented in Eq. 1 by measuring relative changes in f_{SH} over time. Operationally, a simultaneous measurement of f_{SH} and ν_1 yields the partial derivative $\frac{df_{\text{SH}}}{d\nu_1} \approx \frac{\partial f_{\text{SH}}}{\partial x} \frac{\partial x}{\partial \nu_1}$, where x represents a material property or environmental coupling. Temperature is a particularly relevant coupling for resonators exposed to the ambient environment, as temperature causes a frequency shift proportional to the thermo-optic coefficient. A temperature-induced frequency shift of ν_1 results in

$$\frac{\partial f_{\text{SH}}}{\partial T} \frac{\partial T}{\partial \nu_1} = 1 - \frac{1}{2} \frac{m_2}{m_1} \frac{n_1}{n_2} \left(\frac{\frac{1}{n_2} \frac{dn_2}{dT} + \frac{1}{L} \frac{dL}{dT}}{\frac{1}{n_1} \frac{dn_1}{dT} + \frac{1}{L} \frac{dL}{dT}} \right), \quad (2)$$

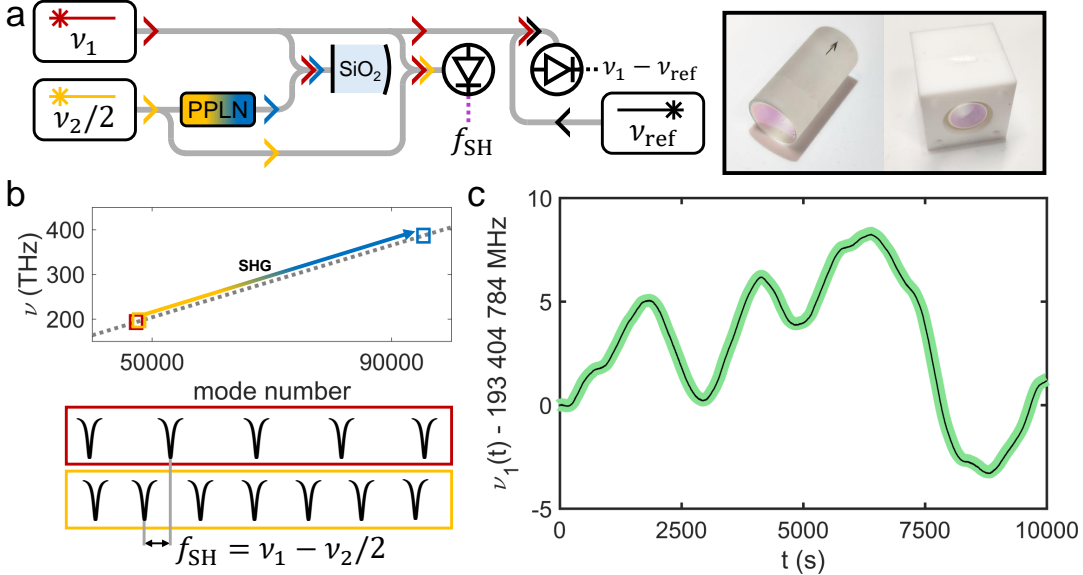


Figure 1: (a) Experimental setup for SH stabilization. One laser at frequency ν_1 directly locks to the dispersive resonator, and the other at frequency $\nu_2/2$ is first frequency-doubled using periodically poled lithium niobate (PPLN) to ν_2 before locking to the resonator. An additional reference laser, ν_{ref} , is used for out-of-loop characterization. The fused silica Fabry-Perot resonator is shown to the right. (b) Resonant mode structure diagram defining f_{SH} with modes highlighted around ν_1 (red), $\nu_2/2$ (yellow), and ν_2 (blue). (c) Demonstration of the correlation between changes in f_{SH} and changes in absolute resonant frequency. The green band shows resonant frequency fluctuations characterized with the external reference laser, and the black line shows fluctuations in f_{SH} scaled by a constant factor of $1/(-48.7)$.

including frequency-dependence of the thermo-optic coefficient. The Sellmeier index of refraction for fused silica [29] at $\nu_1 = 193\,404\,610 \pm 20$ MHz and $\nu_2 = 386\,806\,800 \pm 40$ MHz and previously reported values for $d\text{n}(\nu)/dT$ [30, 31] and $(1/L)dL/dT$ [32] predict a scaling of $1/(-48 \pm 2)$, which agrees with our calibration. Expanding on this result, we note that other environmental conditions can couple to the magnitude of the scaling factor in a similar manner. Vibration, pressure, and humidity all plausibly have frequency-dependent material couplings analogous to the thermo-optic coefficient [33, 34], and a similar derivation to Eq. 2 can yield those contributions.

3 Characterization of f_{SH}

Since f_{SH} is a microwave signal that directly relates the frequency of our resonator-stabilized laser, we explore the effects of noise and offsets in the PDH measurement systems; see Fig. 2. The microwave spectrum of f_{SH} (Fig. 2a, top) demonstrates a narrow-linewidth signal with high signal-to-noise ratio for precision frequency metrology. We examine the frequency noise power spectral density (FN PSD; Fig. 2a, bottom) of f_{SH} (magenta) and its two lasers (red, yellow). Using the PSD, we calculate $1/\pi$ integral linewidths for f_{SH} , ν_1 , and $\nu_2/2$ to be 16 Hz, 35 Hz, and

36 Hz, respectively. At $10^2 - 10^3$ Hz offset from carrier, the individual lasers feature frequency noise with a PSD of $10^0 - 10^1$ Hz 2 /Hz due to thermorefractive noise of the photonic resonator, consistent with photonic resonator thermal noise [13, 15]. For offset frequency above 400 Hz, the white frequency noise spectrum of the PDH-locked lasers is approximately 4×10^{-1} Hz 2 /Hz. On f_{SH} , we see the quadrature sum of the lasers' white noise. The white noise therefore sets a fundamental noise floor in our implementation of this technique, although residual technical noise limits our results in practice. Using f_{SH} to infer frequency fluctuations in ν_1 requires multiplying by the reciprocal of the scaling factor, $1/(df_{\text{SH}}/d\nu_1)$; when f_{SH} is scaled by our calibrated factor, the white noise floor becomes $\sim 10^3$ Hz 2 /Hz. Laser dynamics with a frequency noise PSD below this level are impossible to infer from f_{SH} . Because high-offset-frequency noise of the laser falls below this level, our implementation of this technique cannot infer the short-term stability of the resonator-stabilized laser.

A long-duration measurement of f_{SH} is susceptible to residual technical noise that degrades the accuracy of drift inference. We further detail our experimental setup with SH stabilization, highlighting the methods used to minimize residual technical noise that affects f_{SH} , in Fig. 2b.

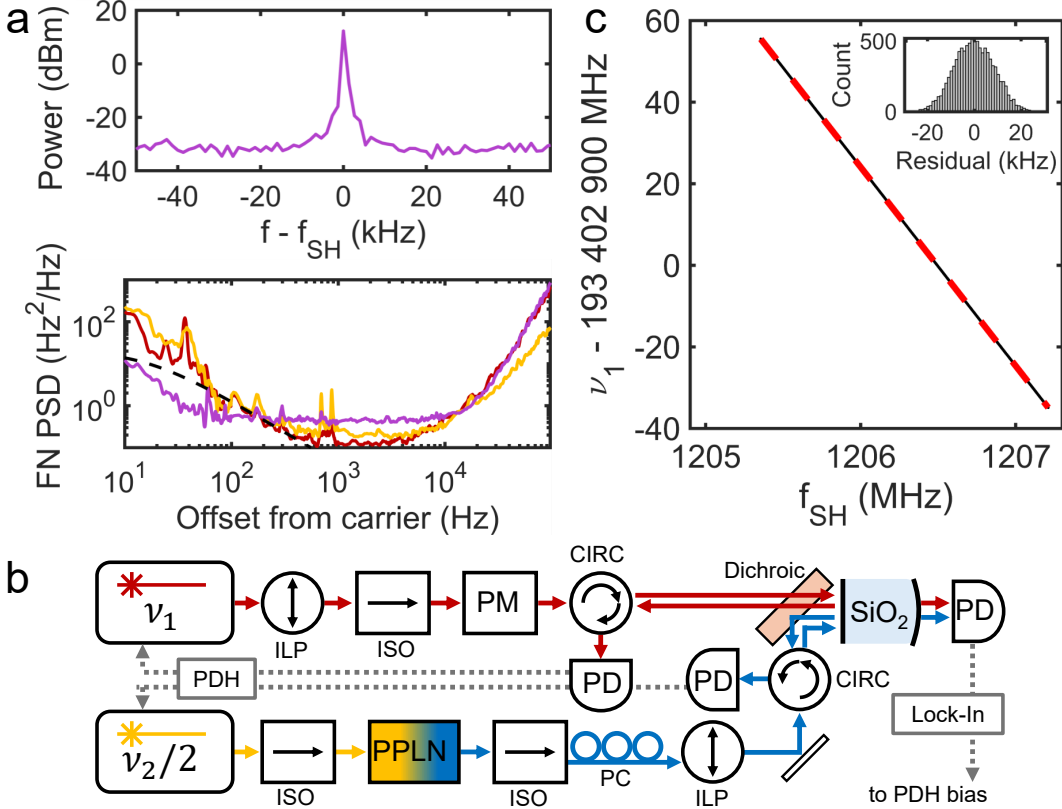


Figure 2: (a) Top: spectrum of f_{SH} ; bottom: frequency noise power spectral density (FN PSD) for ν_1 (red), $\nu_2/2$ (yellow), and f_{SH} (magenta). Theoretical estimate of thermal noise is shown in dashed black. (b) System diagram for our experiment. Gray lines represent feedback loops including PDH locking and transmission lock-in detection. ILP: in-line polarizer, ISO: isolator, PM: phase modulator, CIRC: circulator, PD: photodetector, PPLN: periodically poled lithium niobate, PC: polarization control. (c) Thermal transient measurement of the scaling factor between f_{SH} and ν_1 , $df_{\text{SH}}/d\nu_1$. Linear fit with slope $1/(-48.7 \pm 0.1)$ is shown in dashed red, and residuals to the fit are histogrammed in the upper right inset.

We use polarization-maintaining (PM) fibers and PM-fiber-coupled phase modulators, splitters, isolators, in-line polarizers and circulators to maintain linear polarization with respect to the phase modulator crystal axis and the birefringent polarization states of the resonator [15]. We measure the PDH bias before and after our measurements and observe that the bias shifts slowly over long measurements. We attribute this bias shift to residual amplitude modulation (RAM) [35, 36, 37], which is introduced when polarization noise from the phase modulators used for PDH is passed through polarizing components. Since RAM serves to change the PDH lock bias, we expect transmission through the cavity to vary as the lasers' frequencies change relative to true resonance minima. We include additional lock-in detection on the transmission through the resonator as a slow feedback loop to combat this effect and keep the PDH-locking loop centered on the true resonance minimum. With this, we see a reduction

in PDH bias drift, however it still remains at a small but significant level. While our system includes efforts to minimize RAM-induced PDH bias noise, future work on SH stabilization could aim to further eliminate RAM to realize more accurate measurements of f_{SH} .

Technical noise affects the ability to infer ν_1 using f_{SH} at a level depending on $df_{\text{SH}}/d\nu_1$. We directly measure $df_{\text{SH}}/d\nu_1$ by adjusting the resonator enclosure temperature setpoint and simultaneously recording the frequencies of f_{SH} and the out-of-loop reference heterodyne during equilibration. By changing the temperature, we establish conditions in which thermal gradients dominate over pressure, humidity, and vibrations, thereby satisfying the assumption of a temperature-induced frequency change made in Eq. 2. We apply a change of $+0.1^\circ\text{C}$, recording a frequency shift of approximately -100 MHz for ν_1 and $+2\text{ MHz}$ for f_{SH} over $1,000\text{ s}$. We plot this in Fig. 2c alongside a linear fit and a histogram of the fit residuals. Using this fit,

we determine $df_{\text{SH}}/d\nu_1$ to be $1/(-48.7 \pm 0.1)$. The uncertainty in this measurement is dominated by the effects of technical noise in the system, including RAM, but also includes the influences of other environmental effects not accounted for in the approximation $\frac{df_{\text{SH}}}{d\nu_1} \approx \frac{\partial f_{\text{SH}}}{\partial T} \frac{\partial T}{\partial \nu_1}$. We find the correlation to be exceptionally linear ($R^2 > 1 - 10^{-7}$), suggesting that the further reduction in these remaining sources of uncertainty can lead to a significantly more precise measurement of the scaling factor. This measurement is consistent with the calibrated value found in Fig. 1c for steady-state exposure, suggesting that our ambient conditions sufficiently satisfy the assumptions of Eq. 2.

4 Frequency Drift Inference

To explore the applicability of SH stabilization in improving long-term stability, we measure the accuracy of inferring frequency drift with f_{SH} ; see Fig. 3. We simultaneously record f_{SH} and the out-of-loop reference heterodyne during steady-state environmental conditions for times up to 10,000 s (Fig. 3a). To infer fluctuations in ν_1 , we scale fluctuations in f_{SH} by our calibrated factor of $1/(-48.7)$. We then take the difference between this scaled f_{SH} and the reference heterodyne to create a residual signal that we use to characterize the inference's accuracy.

We find that SH stabilization infers drift to the Hz/s level, with further precision limited by the residual technical noise in our system. We plot experimental data for a measurement period of 4,000 s in Fig. 3a. We plot the corresponding residual signal in Fig. 3b and include a linear fit as a characterization of any residual drift. We see that although short-term fluctuations are increased by the scaling factor, the drift of 6.5 kHz/s is accurately inferred with the residual featuring a drift of only -2.3 Hz/s. We also include the residual signal for two longer measurements of 10,000 s in Fig. 3c. For these longer measurements, we find a residual frequency drift of 7 Hz/s (purple) and 3 Hz/s (pink). Based on our system characterization, we attribute this level of residual drift to the effects of RAM. As the phase modulators and PM fiber slowly change temperature, the magnitude of RAM affecting each laser varies. Accordingly, the changing PDH bias offsets cause f_{SH} to exhibit a slow frequency drift unrelated to resonator dynamics. Without RAM, we expect the long term stability to be limited by the scaled flicker floor arising from technical noise in laser stabilization electronics, which dominates the noise PSD at low frequency offsets. We estimate this flicker noise to contribute 5×10^3 Hz²/Hz to the frequency noise PSD of f_{SH} at 1 Hz offset, which corresponds to a fractional frequency stability of the resonator-stabilized laser of 2×10^{-11} at all averaging times after scaling by our calibrated factor.

To summarize fluctuations in ν_1 and the inference pro-

vided by f_{SH} , we plot the Allan deviation of the free-running laser and the residual signals in Fig. 3c. Over the plotted range of offset frequencies, the Allan deviation of the free-running resonator (black line) features τ^1 dependence characteristic of frequency drift with a magnitude of 6.5 kHz/s. At averaging times less than 300 s, the stability of the residual signals (colors corresponding to Fig. 3b,c) is limited by the scaled flicker noise, while the residual drift begins to dominate at longer averaging times. At an averaging time of 1,000 s, the residual signals exhibit fractional frequency stability in the range of $1 - 3 \times 10^{-11}$. Compared to the free-running resonator, which has a stability of 2×10^{-8} at 1,000 s, this represents a three order of magnitude improvement. In Fig. 3, we include a power-law summary of different experimental measurements (gray dashed line), featuring a scaled flicker floor with frequency noise PSD of $(48.7)^2 \times 5 \times 10^3$ Hz²/Hz at 1 Hz offset and a residual linear drift of 3 Hz/s. We omit the limit set by scaled white noise in this plot because it falls significantly below the effects of flicker noise and remaining drift, although it would pose an ultimate limit should these other contributions be reduced.

5 Conclusion

We have demonstrated SH stabilization as a technique that accurately infers frequency drift in a dispersive resonator to the Hz/s level. Leveraging energy conservation in SHG, our system realizes SH stabilization using two lasers locked to the resonator. We show that the fluctuations in f_{SH} accurately infer corresponding fluctuations in absolute resonant frequencies, related by a material-defined scaling factor. We both calibrate and directly measure this factor, finding a consistent value that agrees with a theoretical estimate leveraging previously reported properties of the resonator material. We also examine the limits of SH stabilization in its inference of resonant frequency fluctuations by analyzing the effects of fundamental and excess sources of noise, including thermo-refractive noise, shot noise, and RAM introduced in the PDH-locking scheme. Because the residual drift and uncertainty in the scaling factor are consistent with the effects of RAM, we identify the further elimination of RAM as a focal point in future precision experiments involving SH stabilization.

Another avenue for further exploration into SH stabilization is in applying the frequency drift inference for active frequency control, e.g. feedforward or feedback. We first note that, while applying the scaling factor to infer drift from a measured f_{SH} is in-loop and does not require an independent reference, the calibration of the scaling factor we performed does require a more stable reference. One possibility for a system that applies SH stabilization would be to undergo an initial calibration period to de-

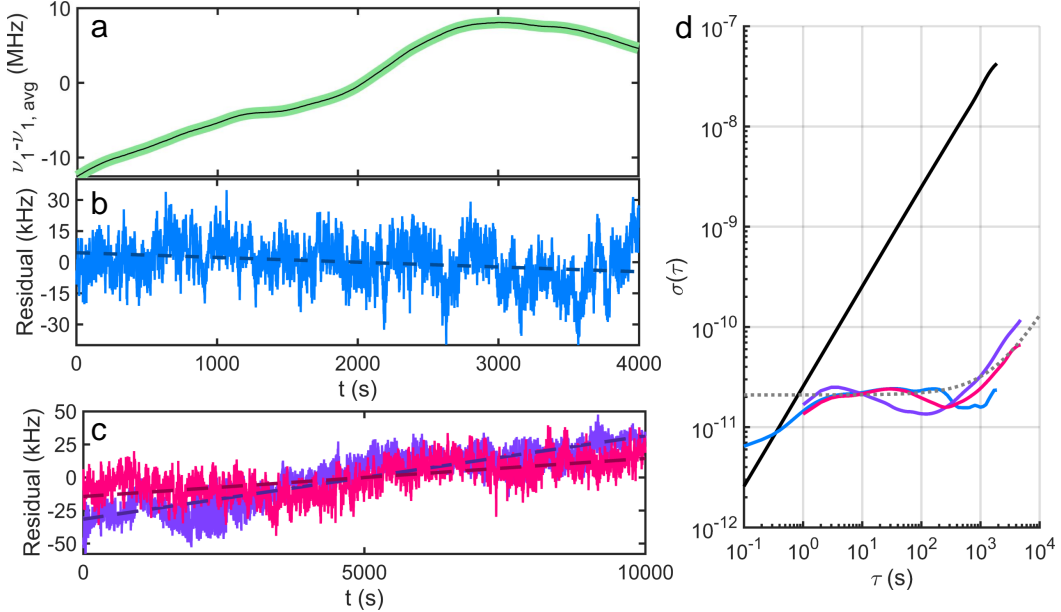


Figure 3: (a) Comparison of true optical deviation derived from external reference laser (green band) and scaled f_{SH} (black line). (b) Residual of truth signal and scaled f_{SH} . Dashed line shows linear fit for residual frequency drift. (c) Residuals for two longer data sets and their resulting linear drift fits. (d) Allan deviation for original optical signal shown in black. Allan deviations for the residual signals in panels b and c are plotted in their respective colors. An approximate power-law summary is included in dashed gray featuring 3 Hz/s linear drift and flicker noise that contributes $(-48.7)^2 \times 5 \times 10^3 \text{ Hz}^2/\text{Hz}$ to the frequency noise PSD at 1 Hz offset.

termine the scaling factor, analogous to the calibration in Fig. 1c or the direct measurement in Fig. 2c. Such an implementation could suffer from inaccuracy if environmental conditions shift and the actual scaling factor changes from the calibrated value, likely prompting recalibration if the changes are significant and persistent. Perhaps the most compelling method of applying SH stabilization would be in the case of an in-situ, external-reference-free measurement of the scaling factor. This could involve modulating the cavity and examining how f_{SH} responds, thus conveying the scaling factor. Such a method to modulate the cavity in a known fashion without relying on an external reference remains an open challenge, but a solution could herald the robust and practical implementation of SH stabilization.

Looking forward, SH stabilization provides a compelling technique to infer drift in dispersive resonators. Its application to other form-factors and further application to compact Fabry-Perot geometries could serve to progress practical and scalable resonators to provide stable absolute frequencies with long-term operation in ambient conditions. Such advancement would support the evolution of precision metrology in an increasingly wide array of environments.

References

[1] B. J. Bloom et al. “An optical lattice clock with accuracy and stability at the 10^{-18} level”. In: *Nature* 506.7486 (Feb. 2014), pp. 71–75. DOI: 10.1038/nature12941.

[2] T. M. Fortier et al. “Generation of ultrastable microwaves via optical frequency division”. In: *Nature Photonics* 5.7 (July 2011), pp. 425–429. DOI: 10.1038/nphoton.2011.121.

[3] H. Al-Taiy et al. “Ultra-narrow linewidth, stable and tunable laser source for optical communication systems and spectroscopy”. In: *Optics Letters* 39.20 (Oct. 2014), pp. 5826–5829. DOI: 10.1364/OL.39.005826.

[4] T. Kessler et al. “A sub-40-mHz-linewidth laser based on a silicon single-crystal optical cavity”. In: *Nature Photonics* 6.10 (Oct. 2012), pp. 687–692. DOI: 10.1038/nphoton.2012.217.

[5] D. G. Matei et al. “1.5 μm Lasers with Sub-10 mHz Linewidth”. In: *Physical Review Letters* 118.26 (June 2017), p. 263202. DOI: 10.1103/PhysRevLett.118.263202.

[6] John M. Robinson et al. “Crystalline optical cavity at 4 K with thermal-noise-limited instability and ultralow drift”. In: *Optica* 6.2 (Feb. 2019), pp. 240–243. DOI: 10.1364/OPTICA.6.000240.

[7] Eugen Wiens et al. “A simplified cryogenic optical resonator apparatus providing ultra-low frequency drift”. In: *Review of Scientific Instruments* 91.4 (Apr. 2020), p. 045112. DOI: 10.1063/1.5140321.

[8] Jamie A. Boyd and Thierry Lahaye. “A basic introduction to ultrastable optical cavities for laser stabilization”. In: *American Journal of Physics* 92.1 (Jan. 2024), pp. 50–58. DOI: 10.1119/5.0161369.

[9] Ying Liu et al. “Cavity ring-down spectroscopy with a laser frequency stabilized and locked to a reference target gas absorption for drift-free accurate gas sensing measurements”. In: *Frontiers in Physics* 11 (July 2023). DOI: 10.3389/fphy.2023.1238869.

[10] G. Giorgi et al. “Advanced technologies for satellite navigation and geodesy”. In: *Advances in Space Research* 64.6 (Sept. 2019), pp. 1256–1273. DOI: 10.1016/j.asr.2019.06.010.

[11] A. E. Shitikov et al. “Billion Q-factor in silicon WGM resonators”. In: *Optica* 5.12 (Dec. 2018), pp. 1525–1528. DOI: 10.1364/OPTICA.5.001525.

[12] Shancheng Yang, Yue Wang, and Handong Sun. “Advances and Prospects for Whispering Gallery Mode Microcavities”. In: *Advanced Optical Materials* 3.9 (2015), pp. 1136–1162. DOI: 10.1002/adom.201500232.

[13] Wei Zhang et al. “Microrod Optical Frequency Reference in the Ambient Environment”. In: *Physical Review Applied* 12.2 (Aug. 2019), p. 024010. DOI: 10.1103/PhysRevApplied.12.024010.

[14] Matthew W. Puckett et al. “422 Million intrinsic quality factor planar integrated all-waveguide resonator with sub-MHz linewidth”. In: *Nature Communications* 12.1 (Feb. 2021), p. 934. DOI: 10.1038/s41467-021-21205-4.

[15] Wei Zhang et al. “Ultranarrow Linewidth Photonic-Atomic Laser”. In: *Laser & Photonics Reviews* 14.4 (2020), p. 1900293. DOI: 10.1002/lpor.201900293.

[16] Wei Zhang et al. “Monolithic optical resonator for ultrastable laser and photonic millimeter-wave synthesis”. In: *Communications Physics* 7.1 (June 2024), pp. 1–6. DOI: 10.1038/s42005-024-01660-3.

[17] Haotian Cheng et al. “Harnessing micro-Fabry-Pérot reference cavities in photonic integrated circuits”. In: *Nature Photonics* (June 2025), pp. 1–7. DOI: 10.1038/s41566-025-01701-5.

[18] R X Adhikari et al. “A cryogenic silicon interferometer for gravitational-wave detection”. In: *Classical and Quantum Gravity* 37.16 (July 2020), p. 165003. DOI: 10.1088/1361-6382/ab9143.

[19] J. Alnis et al. “Subhertz linewidth diode lasers by stabilization to vibrationally and thermally compensated ultralow-expansion glass Fabry-P’erot cavities”. In: *Physical Review A* 77.5 (May 2008), p. 053809. DOI: 10.1103/PhysRevA.77.053809.

[20] Isao Ito et al. “Stable CW laser based on low thermal expansion ceramic cavity with 4.9 mHz/s frequency drift”. In: *Optics Express* 25.21 (Oct. 2017), pp. 26020–26028. DOI: 10.1364/OE.25.026020.

[21] Wei Zhang et al. *Cryogenic photonic resonator with $10^{-17}/\text{s}$ drift*. arXiv:2410.09960 [physics]. Oct. 2024. DOI: 10.48550/arXiv.2410.09960.

[22] D. V. Strekalov et al. “Temperature measurement and stabilization in a birefringent whispering gallery mode resonator”. In: *Optics Express* 19.15 (July 2011), pp. 14495–14501. DOI: 10.1364/OE.19.014495.

[23] I. Fescenko et al. “Dual-mode temperature compensation technique for laser stabilization to a crystalline whispering gallery mode resonator”. In: *Optics Express* 20.17 (Aug. 2012). Publisher: Optica Publishing Group, pp. 19185–19193. DOI: 10.1364/OE.20.019185.

[24] L. M. Baumgartel, R. J. Thompson, and N. Yu. “Frequency stability of a dual-mode whispering gallery mode optical reference cavity”. In: *Optics Express* 20.28 (Dec. 2012), pp. 29798–29806. DOI: 10.1364/OE.20.029798.

[25] Jinkang Lim et al. “Probing 10 μK stability and residual drifts in the cross-polarized dual-mode stabilization of single-crystal ultrahigh-Q optical resonators”. In: *Light: Science & Applications* 8.1 (Jan. 2019), p. 1. DOI: 10.1038/s41377-018-0109-7.

[26] Qiancheng Zhao et al. “Integrated reference cavity with dual-mode optical thermometry for frequency correction”. In: *Optica* 8.11 (Nov. 2021), pp. 1481–1487. DOI: 10.1364/OPTICA.432194.

[27] Wenle Weng et al. “Nano-Kelvin Thermometry and Temperature Control: Beyond the Thermal Noise Limit”. In: *Physical Review Letters* 112.16 (Apr. 2014). Publisher: American Physical Society, p. 160801. DOI: 10.1103/PhysRevLett.112.160801.

[28] R. W. P. Drever et al. “Laser phase and frequency stabilization using an optical resonator”. In: *Applied Physics B* 31.2 (June 1983), pp. 97–105. DOI: 10.1007/BF00702605.

[29] I. H. Malitson. “Interspecimen Comparison of the Refractive Index of Fused Silica*,†”. In: *JOSA* 55.10 (Oct. 1965), pp. 1205–1209. DOI: 10.1364/JOSA.55.001205.

[30] Douglas B. Leviton and Bradley J. Frey. “Temperature-dependent absolute refractive index measurements of synthetic fused silica”. In: ed. by Eli Atad-Ettedgui, Joseph Antebi, and Dietrich Lemke. Orlando, Florida, USA, June 2006, 62732K. DOI: 10.1117/12.672853.

[31] Gaspar Rego. “Temperature Dependence of the Thermo-Optic Coefficient of SiO₂ Glass”. In: *Sensors* 23.13 (Jan. 2023), p. 6023. DOI: 10.3390/s23136023.

[32] J. W. Berthold and S. F. Jacobs. “Ultraprecise thermal expansion measurements of seven low expansion materials”. In: *Applied Optics* 15.10 (Oct. 1976), p. 2344. DOI: 10.1364/AO.15.002344.

[33] A. Bertholds and R. Dandliker. “Determination of the individual strain-optic coefficients in single-mode optical fibres”. In: *Journal of Lightwave Technology* 6.1 (Jan. 1988), pp. 17–20. DOI: 10.1109/50.3956.

[34] Hao Sun et al. “An Optical Fiber Fabry–Perot Interferometer Sensor for Simultaneous Measurement of Relative Humidity and Temperature”. In: *IEEE Sensors Journal* 15.5 (May 2015), pp. 2891–2897. DOI: 10.1109/JSEN.2014.2383387.

[35] N. C. Wong and J. L. Hall. “Servo control of amplitude modulation in frequency-modulation spectroscopy: demonstration of shot-noise-limited detection”. In: *Journal of the Optical Society of America B* 2.9 (Sept. 1985), p. 1527. DOI: 10.1364/JOSAB.2.001527.

[36] Edward A. Whittaker, Manfred Gehrtz, and Gary C. Bjorklund. “Residual amplitude modulation in laser electro-optic phase modulation”. In: *Journal of the Optical Society of America B* 2.8 (Aug. 1985), p. 1320. DOI: 10.1364/JOSAB.2.001320.

[37] W. Zhang et al. “Reduction of residual amplitude modulation to 1×10^{-6} for frequency modulation and laser stabilization”. In: *Optics Letters* 39.7 (Apr. 2014), p. 1980. DOI: 10.1364/OL.39.001980.

6 Methods

Measurements of f_{SH}

We measure f_{SH} by first passing the microwave heterodyne signal produced by a photodiode through a frequency divider, dividing the ~ 1 GHz f_{SH} by 32 so that it is within the bandwidth of our frequency counter (Keysight 53230a). We synchronize two counters to measure both the $\nu_1 - \nu_{\text{ref}}$ (also divided) and f_{SH} heterodynes simultaneously. For our measurements of 10,000 ($< 10,000$) s, we use a gate time of 1 (0.1) s externally triggered by a waveform generator for synchronization between the two counters; the dead-time between gating periods is 10 (100) μs .

Transmission Lock-in Detection

In the free-space path after transmission through the resonator, we include a dichroic beamsplitter to separate transmission of ν_1 and ν_2 and focus them each onto a photodetector. We apply a lock-in modulation to the DC bias of our PID controllers used for PDH locking. We choose lock-in modulation frequencies that are significantly faster than the apparent drift caused by RAM, which we observe on the order of 1000 s, while also being significantly slower than the bandwidth of the PID controllers. We use two different modulation frequencies for ν_1 and ν_2 that are between 100 and 200 Hz, avoiding integer multiples of 60 Hz. By using a slow feedback loop from the lock-in amplifier (SRS SR830 DSP) to maximize the transmission amplitude, the laser is, on average, centered on the cavity resonance despite possible DC bias offsets caused by RAM. Although the lock-in modulation means the laser may instantaneously be off-resonance, the relatively high modulation frequency and its single-frequency nature means we can still accurately infer drift using the the average laser frequencies.

7 Acknowledgements

We thank Aidan Jones and Sarang Yeola for careful review of the manuscript.

Funding: This research has been funded by AFOSR FA9550-20-1-0004 Project Number 19RT1019, NSF Quantum Leap Challenge Institute Award OMA – 2016244, and NIST.

Competing interests: The authors declare no competing interests. This work is a contribution of the US Government and is not subject to US copyright. Mention of specific companies or trade names is for scientific communication only and does not constitute an endorsement by NIST.

Data and materials availability: All data necessary to support the claims within the paper are included in the plots. Reasonable requests for numeric data will be honored.